Supporting Information

NH Bond Activation of Ammonia and Amines by Ditetrelenes: Key Insights into the Stereochemistry of Nucleophilic Addition

Sarah L. McOnie, Gül Altınbaş Özpinar,* Jeremy L. Bourque, Thomas Müller and Kim M. Baines*

Table of Contents

Experimental

General Considerations

All manipulations were performed under an inert atmosphere of argon using Schlenk techniques or under an atmosphere of nitrogen in an MBraun glovebox. Solvents were purified using an Innovative Technologies 400-5 Solvent Purification System and were stored over activated 4 Å molecular sieves. C_6D_6 was dried over activated 4 Å molecular sieves. Liquid amines were degassed and stored over 4 Å molecular sieves prior to use. Ammonia was

purchased as a 0.4 M solution in THF and dimethylamine was purchased as a 2.0 M solution in THF and used as received. $(Me_3Si)_2SiMes_2$[1] and Ge_3Mes_6[2] were synthesized according to the literature procedure. Tetramesityldisilene, **1**,[1] and tetramesityldigermene, **2**,[3] were synthesized prior to each reaction in quantitative yield. The volatiles were removed and **1/2** were dissolved in the reaction solvent. All other chemicals were purchased from commercial sources and used without further purification.

All new compounds were characterized by ^{1}H, ^{13}C, ^{1}H-^{1}H gCOSY, ^{1}H-^{13}C gHSQC, ^{1}H-^{13}C gHMBC NMR spectroscopy, ESI mass spectrometry and in some cases ^{1}H-^{29}Si gHMBC and ^{1}H-^{15}N gHMBC NMR spectroscopy and X-ray diffraction. NMR spectra were recorded on an Inova 600 MHz NMR spectrometer using C_6D_6 as the solvent at room temperature. The NMR standards used are as follows: ^{1}H NMR spectra were referenced to residual C_6D_5H (7.15 ppm); ^{13}C NMR spectra were referenced to the central transition of C_6D_6 (128.06 ppm); ^{29}Si NMR spectra were referenced to external TMS; and CH_3NO_2 was used as the external standard for ^{15}N NMR spectra. All NMR assignments were confirmed using two-dimensional techniques (gCOSY, gHSQC, gHMBC). Electrospray ionization mass spectra were collected using a Bruker micrOTOF II spectrometer. Mass spectral data are reported in mass-to-charge units (*m/z*).

Preparation of Disilylamines 3-7:

Ammonia (0.3 mL of a 0.4 M solution in THF, 0.12 mmol) was added to was added to a bright yellow solution of tetramesityldisilene, **1**, (64 mg, 0.12 mmol) dissolved in benzene (3 mL) at room temperature. After 10 minutes, the colour of the solution had faded to pale yellow and the solvent was evaporated to yield a pale, yellow oil. Dimethylamine (0.1 mL of a 2.0 M solution in THF, 0.2 mmol) was added to a bright yellow solution of tetramesityldisilene, **1**, (64 mg, 0.12 mmol) dissolved in benzene (3 mL) at room temperature. The solution was allowed to stir for 2 days, after which time the colour of the solution had faded to pale yellow. The product was purified by thin layer chromatography using a silica plate with a fluorescent indicator and a mixture of hexanes and DCM (70:30) as the eluent. The remaining amines (0.12 mmol) were added directly to a bright yellow solution of tetramesityldisilene, **1**, (64 mg, 0.12 mmol) dissolved in benzene (3 mL) at room temperature. Once the colour of the solution had faded to pale yellow (10 minutes for primary amines, 2 days for secondary amines), the solvent was evaporated to yield a pale-yellow oil. Attempts were made to purify the products by thin layer

chromatography using a silica plate with a fluorescent indicator and a mixture of hexanes and DCM (70:30) as the eluent; however, only **6** and **7** could be isolated cleanly from the plates.

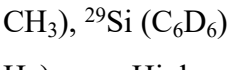

3: Pale, yellow oil (67 mg, 94%) ^{1}H NMR (600 MHz, C_6D_6) 6.75 (s, 4H, *m*-H), 6.69 (s, 4H, *m*-H), 5.64 (s, 1H, Si-H), 2.79 (dt, 2H, ^{3}J = 6 Hz, 6 Hz, N-CH_2), 2.41 (br s, 12H, *o*-CH_3), 2.30 (s, 12H, *o*-CH_3), 2.13 (s, 6H, *p*-CH_3), 2.11 (s, 6H, *p*-CH_3), 1.45 (tq, 2H, ^{3}J = 6 Hz, 6 Hz, CH_2), 0.84 (t, 1H, ^{3}J = 6 Hz, N-H), 0.78 (t, 3H, ^{3}J = 6 Hz, CH_3), ^{13}C{^{1}H} (151 MHz, C_6D_6) 145.32 (*o*-C), 144.61 (*o*-C), 138.62 (*p*-C), 138.46 (*p*-C), 134.21 (*i*-C), 132.50 (*i*-C), 129.69 (*m*-C), 129.13 (*m*-C), 46.32 (N-C), 27.26 (CH_2), 24.70 (*o*-CH_3), 24.48 (*o*-CH_3), 21.12 (*p*-CH_3), 21.04 (*p*-CH_3), 11.88 (CH_3), ^{29}Si (C_6D_6) -56.1 (^{1}J = 180 Hz) Si-H), -15.6 (^{3}J = 8 Hz, Si-N), ^{15}N (C_6D_6) -354.7 (^{1}J = 72 Hz) ppm. High resolution ESI-MS *m/z* for $C_{39}H_{53}NNaSi_2^+$ calc. 614.3614, found 614.3604.

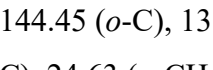

4: Pale yellow oil (65 mg, 92 %) ^{1}H NMR (600 MHz, C_6D_6) 6.75 (s, 4H, *m*-H), 6.69 (s, 4H, *m*-H), 5.65 (s, 1H, Si-H), 3.23 (d of sept, ^{3}J = 8 Hz, 6 Hz, N-CH), 2.43 (s, 12H, *o*-CH_3), 2.27 (s, 12H, *o*-CH_3), 2.13 (s, 6H, *p*-CH_3), 2.11 (s, 6H, *p*-CH_3), 1.02 (d, 6H, ^{3}J = 6 Hz, -CH_3), 0.69 (d, 1H, ^{3}J = 8 Hz, NH), ^{13}C{^{1}H} (151 MHz, C_6D_6) 145.25 (*o*-C), 144.21 (*o*-C), 138.45 (*p*-C), 138.39 (*p*-C), 135.24 (*i*-C), 132.54 (*i*-C), 129.62 (*m*-C), 129.09 (*m*-C), 45.09 (NCH), 27.89 (CH-CH_3), 25.24 (*o*-CH_3), 24.96 (*o*-CH_3), 21.12 (*p*-CH_3), 21.06 (*p*-CH_3), ^{29}Si (C_6D_6) -54.2 (^{1}J = 176 Hz, Si-H), -17.0 (^{1}J = 8 Hz, Si-N) , ^{15}N (C_6D_6) -332.7 (^{1}J = 75 Hz) ppm. High resolution ESI-MS *m/z* for $C_{39}H_{53}NNaSi_2^+$ calc. 614.3614, found 614.3613.

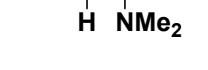

5: Pale yellow oil (61 mg, 92 %) ^{1}H NMR (600 MHz, C_6D_6) 6.73 (s, 4H, *m*-H), 6.68 (s, 4H, *m*-H) 5.67 (s, 1H, Si-H), 2.36, 2.30 (each s, 24H, *o*-CH_3), 2.12 (s, 6H, *p*-CH_3), 2.10 (s, 6H, *p*-CH_3), 0.93 (s, 2H, N-H), ^{13}C{^{1}H} (151 MHz, C_6D_6) 145.39 (*o*-C), 144.45 (*o*-C), 138.56 (*p*-C), 138.54 (*p*-C), 135.50 (*i*-C), 132.16 (*i*-C), 129.76 (*m*-C), 129.17 (*m*-C), 24.63 (*o*-CH_3), 24.44 (*o*-CH_3), 21.12 (*p*-CH_3), 21.02 (*p*-CH_3),^{29}Si (C_6D_6) -54.8 (^{1}J = 176 Hz, Si-H), -17.0 (^{1}J = 8 Hz, Si-N), ^{15}N (C_6D_6) -362.9 (^{1}J = 72 Hz) ppm. High resolution ESI-MS m/z for $C_{36}H_{47}NNaSi_2^+$ calc. 572.3145, found 572.3155.

6: Isolated using TLC (70:30 hex:DCM). Clear oil (15 mg, 22%). ^{1}H NMR (600 MHz, C_6D_6) 6.74 (s, 4H, *m*-H), 6.69 (s, 4H, *m*-H), 5.85 (s, 1H, Si-H), 2.59 (s, 6H, N-CH_3), 2.31, 2.29 (each s, 24H, *o*-CH_3), 2.11, 2.10 (each s, 12H, *p*-CH_3), ^{13}C{^{1}H} (151 MHz, C_6D_6) 145.22 (*o*-C), 144.34 (*o*-C), 138.40 (*p*-C), 138.36 (*p*-C), 137.35 (*i*-C), 133.22

(*i*-C), 129.74 (*m*-C), 129.40 (*m*-C), 42.57 (N-C), 25.02 (*o*-CH_3), 24.43 (*o*-CH_3), 21.07 (*p*-CH_3), 20.96 (*p*-CH_3), ^{29}Si (C_6D_6) -55.5 (^1J = 180 Hz, Si-H), -9.8 (^3J = 8 Hz, Si-N) ppm, ^{15}N (C_6D_6) No signal observed. High resolution ESI-MS $C_{38}H_{51}NNaSi_2^+$ calc. 600.3458, found 600.3454.

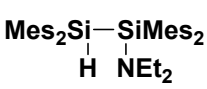

7: Isolated using TLC (70:30 hex:DCM). Clear oil (20 mg, 27 %) ^{1}H NMR (600 MHz, C_6D_6) 6.72 (s, 4H, *m*-H), 6.71 (s, 4H, *m*-H), 5.97 (s, 1H, Si-H), 3.21 (q, ^3J = 6 Hz, 4H, CH_2), 2.35 (s, 24H, *o*-CH_3), 2.11 (s, 6H, *p*-CH_3) , 2.09 (s, 6H, *p*-CH_3), 0.83 (t, ^3J = 6 Hz, 6H, -CH_3), ^{13}C{^{1}H} (151 MHz, C_6D_6) 145.20 (*o*-C), 144.79 (*o*-C), 138.27 (*p*-C), 138.25 (*p*-C) 136.89 (*i*-C), 134.38 (*i*-C), 129.87 (*m*-C), 129.03 (*m*-C), 41.69 (N-C), 25.40 (*o*-CH_3), 25.32 (*o*-CH_3), 21.06 (*p*-CH_3), 20.95 (*p*-CH_3), 12.67 (-CH_3), ^{29}Si (C_6D_6) -53.2 (Si-H), -10.8 (Si-N), ^{15}N (C_6D_6) -354.8 ppm. High resolution ESI-MS m/z for $C_{40}H_{55}NNaSi_2^+$ calc. 628.3771, found 628.3772.

Preparation of Digermylamines 8 and 9:

The amine (0.3 mL of a 0.4 M solution of ammonia in THF or 2 drops of propylamine) was added to a yellow solution of tetramesityldigermene, **2**, (20 mg, 0.03 mmol) dissolved in benzene (3 mL) at room temperature. Once the colour of the solution had faded to pale yellow (10 minutes in each case), the solvent was evaporated to yield a pale-yellow oil. Purification of the crude products by thin layer chromatography using 70:30 hex:DCM as the eluent was attempted; however, only 1,1,2,2-tetramesityldigermanol[4] was recovered from the plate in both reactions. NMR spectra were recorded on the crude products.

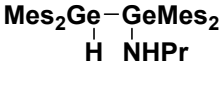

8: ^{1}H NMR (600 MHz, C_6D_6) 6.76 (s, 4H, *m*-H), 6.70 (s, *m*-H), 5.86 (s, 1H, Ge-H), 2.83 (dt, ^3J = 6 Hz, 6 Hz, 2H, N-CH_2), 2.42 (s, *o*-CH_3), 2.34 (s, *o*-CH_3), 2.12 (s, *p*-CH_3), 2.09 (s, *p*-CH_3), 1.52 (tq, ^3J = 6 Hz, 6 Hz, 2H, CH_2), 0.87 (t, ^3J = 6 Hz, 3H, CH_3), 0.77 (br, 1H, N-H), ^{13}C{^{1}H} (151 MHz, C_6D_6) 144.00 (*o*-C), 143.56 (*o*-C), 138.35 (*p*-C), 138.02 (*p*-C), 137.19 (*i*-C), 136.29 (*i*-C), 129.58 (*m*-C), 129.02 (*m*-C), 47.74 (N-CH_2), 28.02 (-CH_2-), 24.85 (*o*-CH_3), 24.21 (*o*-CH_3), 21.06 (*p*-CH_3), 20.99 (*p*-CH_3), 11.89 (-CH_3) ppm. High resolution ESI-MS m/z for $C_{39}H_{53}NNa^{72}Ge^{74}Ge^+$ calc. 704.2508, found 704.2514.

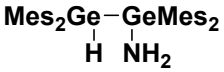

9: sample is contaminated with 1,1,2,2-tetramesityldigermanol (5:1 ratio); ^{1}H NMR (600 MHz, C_6D_6) 6.73 (s, 4H, *m*-H), 6.69 (s, *m*-H), 5.88 (s, 1H, Ge-H), 2.36 (s, *o*-CH_3), 2. 34 (s, *o*-CH_3), 2.12 (s, 6H, *p*-CH_3), 2.10 (s, *p*-CH_3), 0.78 (s, 2H, N-H) ppm. High resolution ESI-MS m/z for $C_{36}H_{47}NNa^{72}Ge^{74}Ge^+$ calc. 662.2039, found 662.2017.

There are two possible sources of 1,1,2,2-tetramesityldigermanol: direct addition of adventitious water to tetramesityldigermene or hydrolysis of **8** (or **9**). Reaction conditions for the formation of **3-7** were similar to those for the formation of **8** and **9**. As no 1,1,2,2-tetramesityldisilanol was observed in the reactions of **1**, which reacts rapidly with H_2O, hydrolysis of the digermene to form the digermanol is unlikely. Thus, the digermanol is likely formed as a result of the hydrolysis of **8** and **9**. This is further supported by the observation that the digermanol is the only product isolated after the crude product mixtures were subjected to thin layer chromatography with undried solvents. In general, germylamines undergo facile hydrolysis.[5] In comparison, silylamines have been shown to be relatively resistant to hydrolysis, with the exception of small (trialkylsilyl)amines,[6] accounting for the successful purification of the disilylamine adducts **6** and **7** using TLC.

NMR Spectra

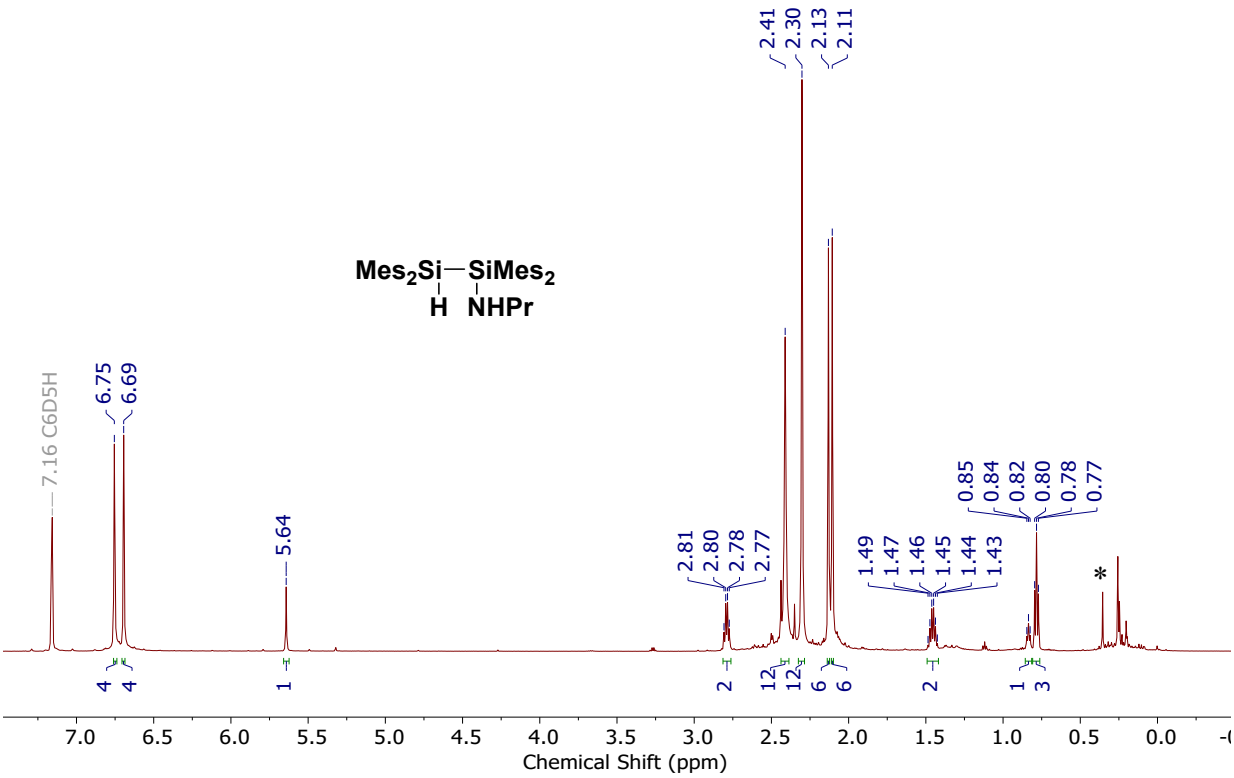

Figure S1 ^{1}H NMR spectrum (600 MHz, C_6D_6) of **3**. The signal denoted by * is trace water. Upfield signals in the spectrum are attributed to trace impurities from the synthesis of **1**.

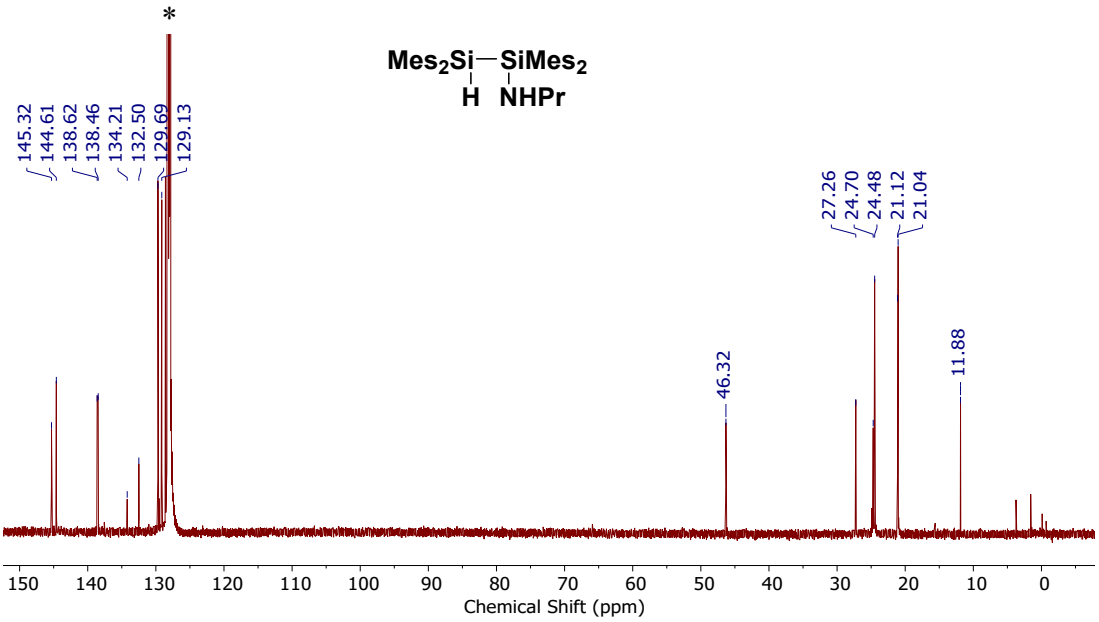

Figure S2 ^{13}C{^{1}H} NMR spectrum (151 MHz, C_6D_6) of **3**. The signal denoted with * is the solvent C_6D_6. The unlabeled upfield peaks are trace impurities from the synthesis of **1**.

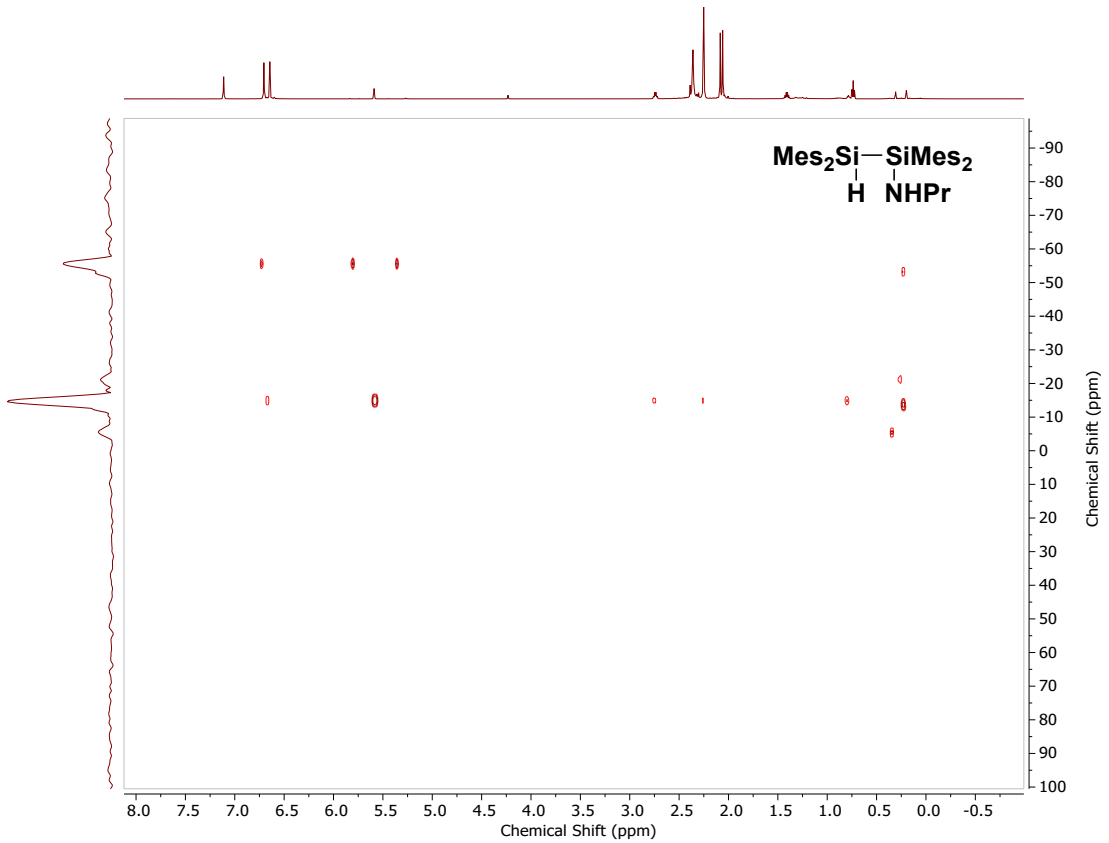

Figure S3 ^{1}H-^{29}Si gHMBC spectrum (C_6D_6) of **3**.

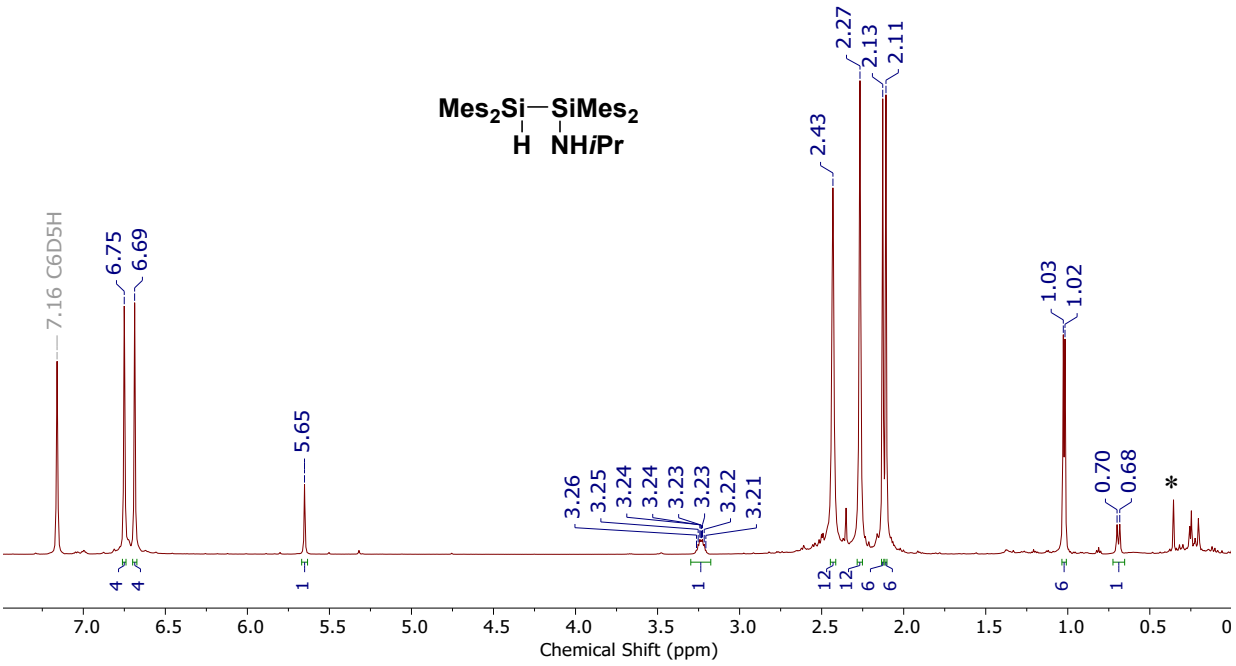

Figure S4 ^{1}H NMR spectrum (600 MHz, C_6D_6) of **4**. The signal denoted with * is trace water. Upfield signals in the spectrum are attributed to trace impurities from the synthesis of **1**.

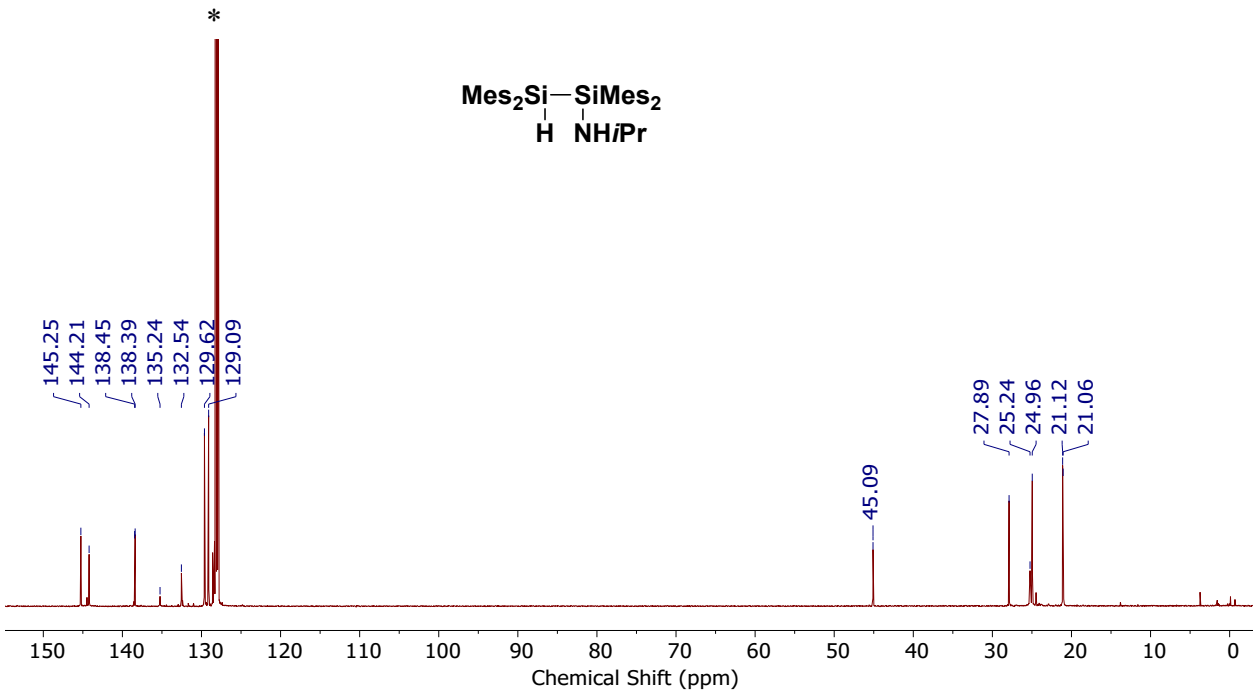

Figure S5 $^{13}C\{^{1}H\}$ NMR spectrum (151 MHz, C_6D_6) of **4**. The signal denoted with * is the solvent C_6D_6.

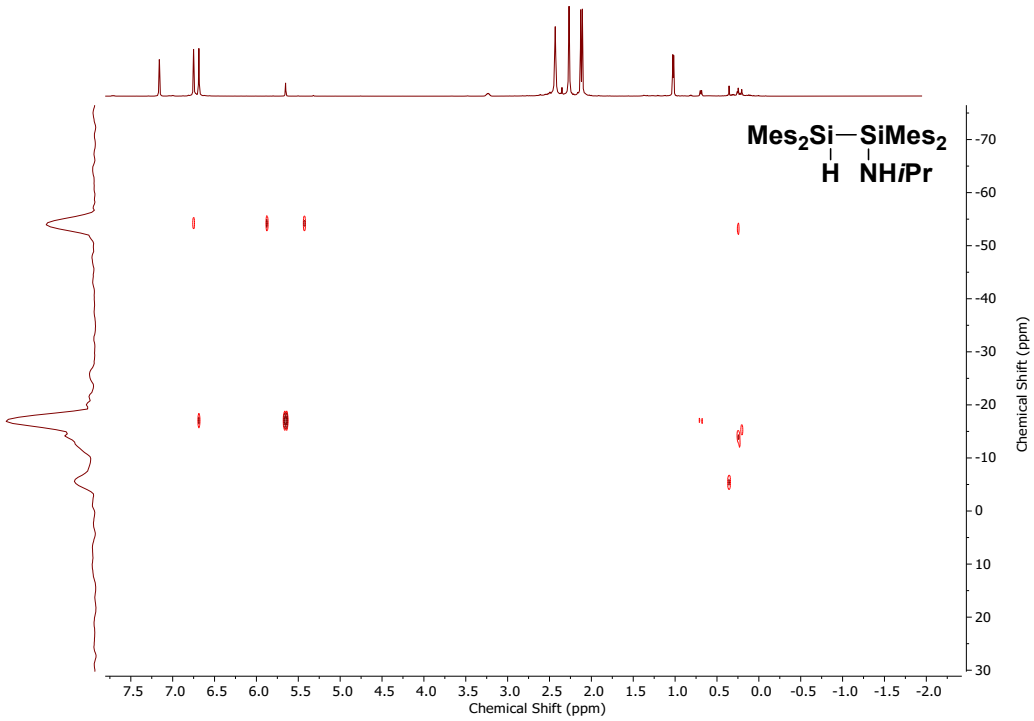

Figure S6 ^{1}H-^{29}Si gHMBC spectrum (C_6D_6) of **4**.

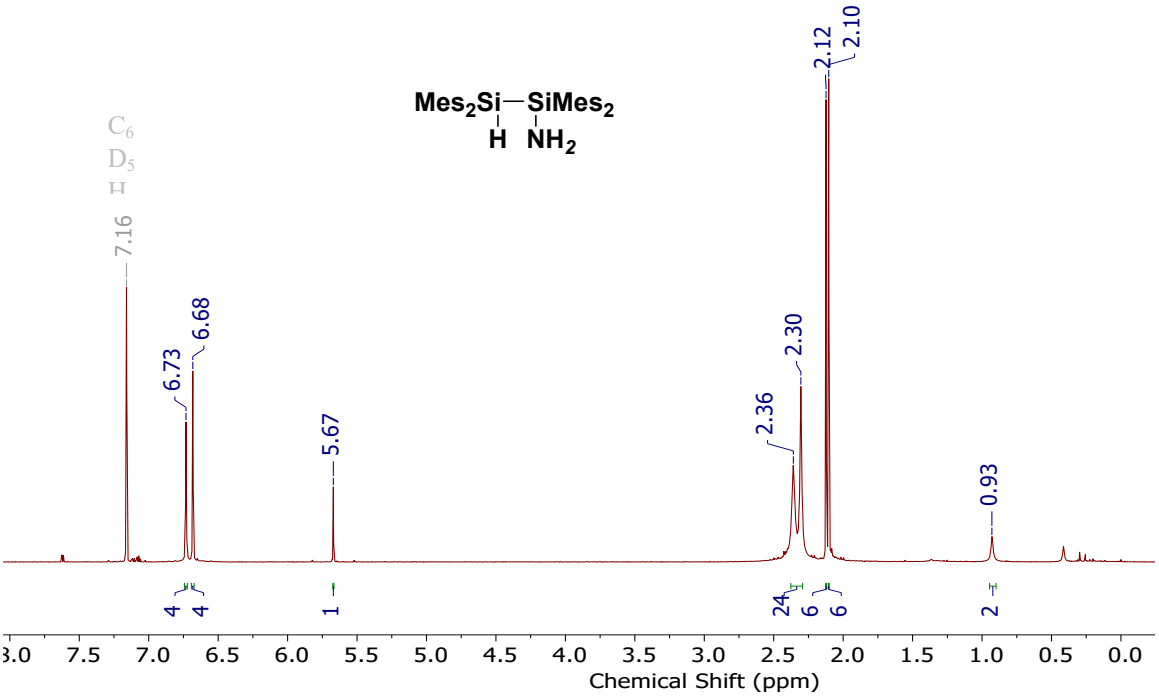

Figure S7 ^{1}H NMR spectrum (600 MHz, C_6D_6) of **5**.

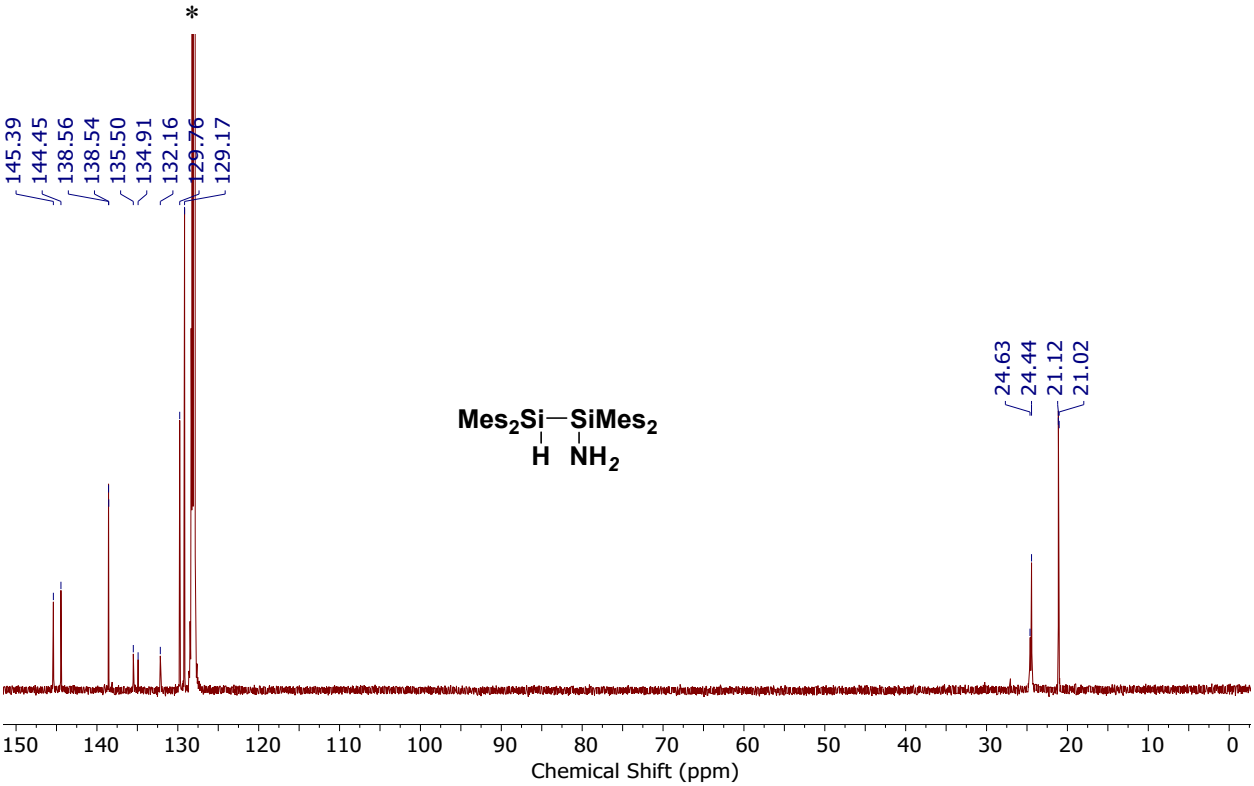

Figure S8 ^{13}C{^{1}H} NMR spectrum (151 MHz, C_6D_6) of **5**. The signal denoted with * is the solvent C_6D_6.

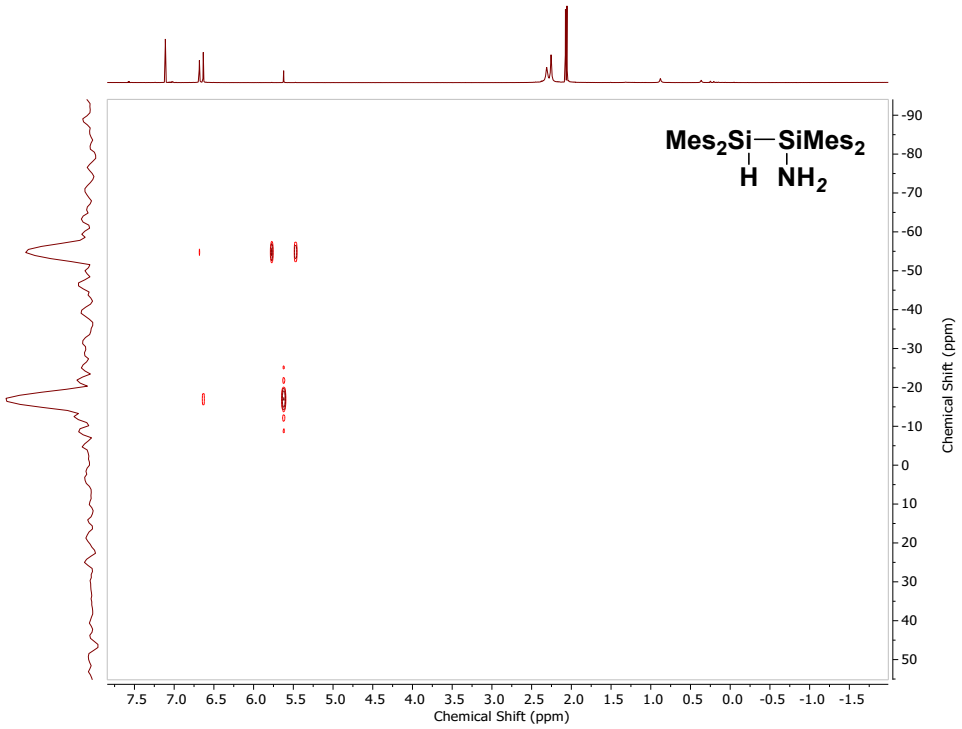

Figure S9 ^{1}H-^{29}Si gHMBC spectrum (C_6D_6) of **5**.

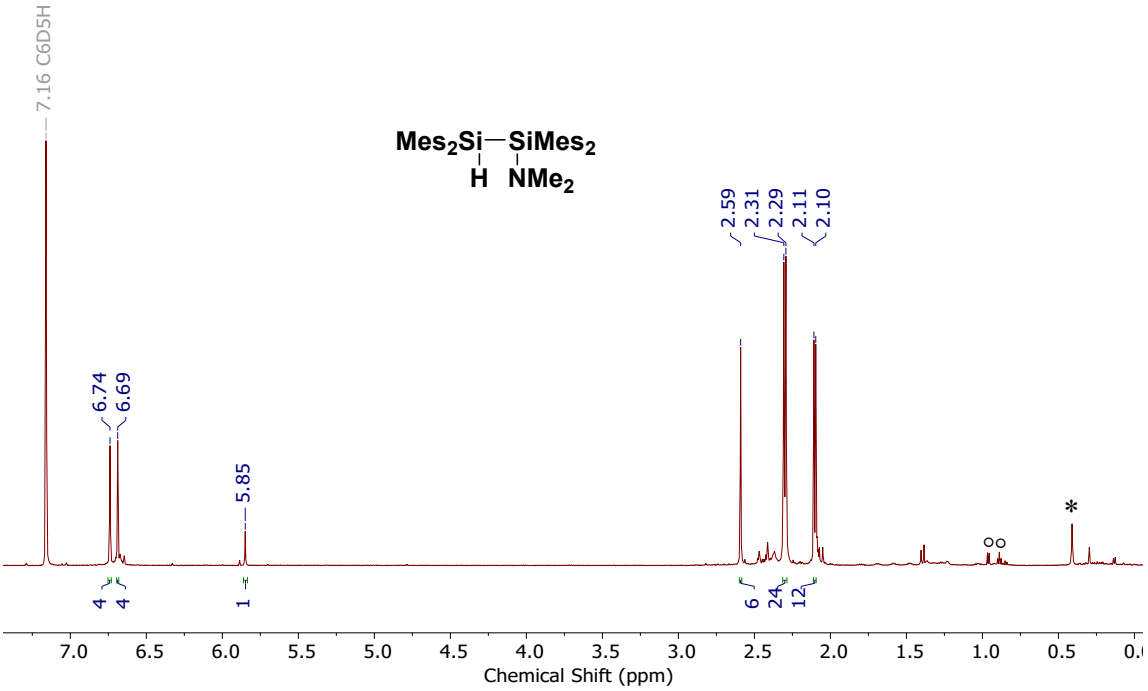

Figure S10 ^{1}H NMR spectrum (600 MHz, C_6D_6) of **6**. The signal denoted with * is trace water. The signal denoted with ° are residual hexanes.

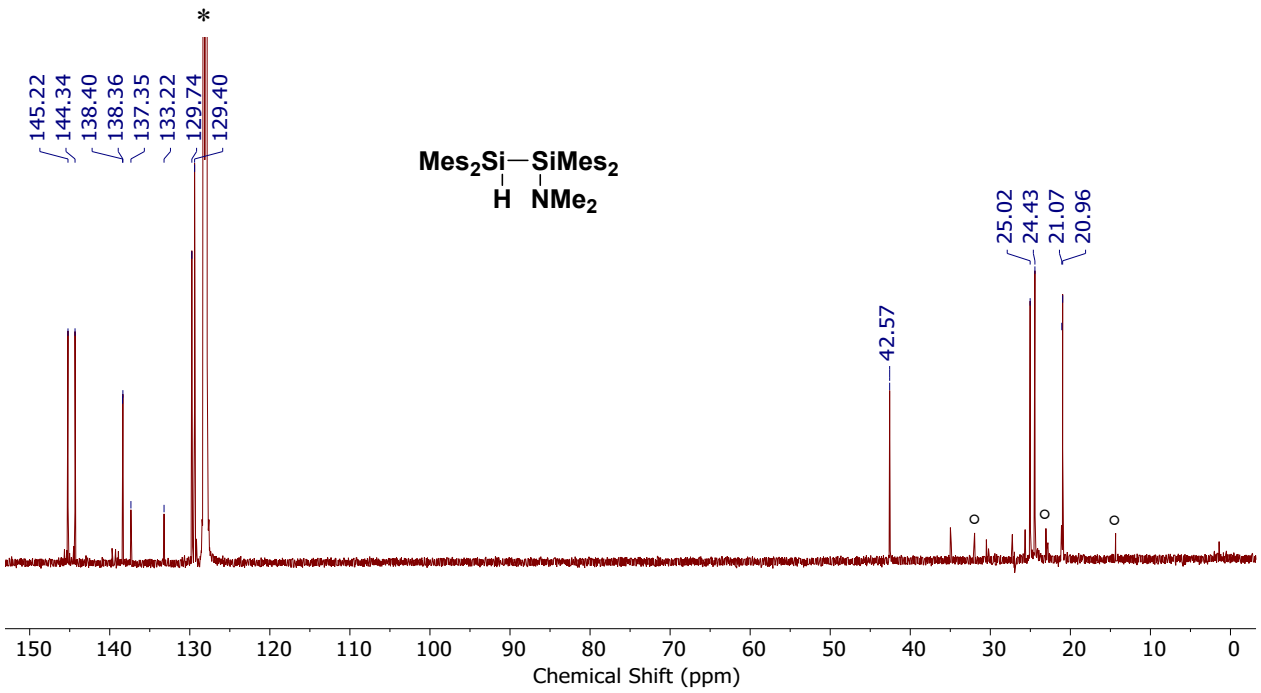

Figure S11 $^{13}C\{^{1}H\}$ NMR spectrum (151 MHz, C_6D_6) of **6**. The signal denoted with * is the solvent C_6D_6. The signals denoted with ° are residual hexanes.

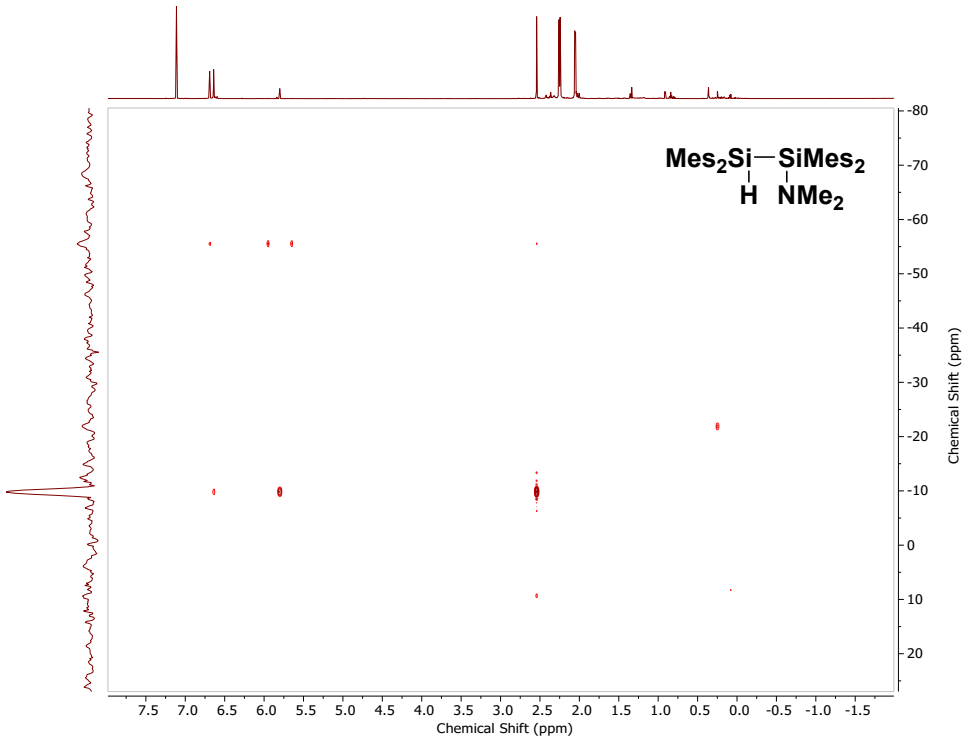

Figure S12 ^{1}H-^{29}Si gHMBC spectrum (C_6D_6) of **6**.

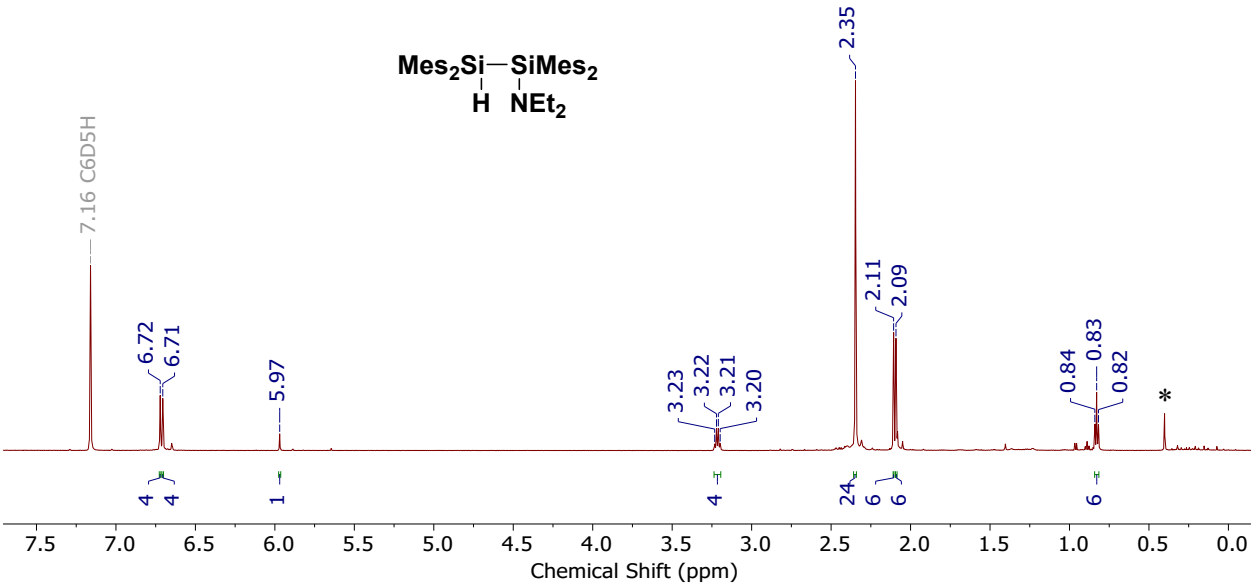

Figure S13 ^{1}H NMR spectrum (600 MHz, C_6D_6) of **7**. The signal denoted with * is trace water.

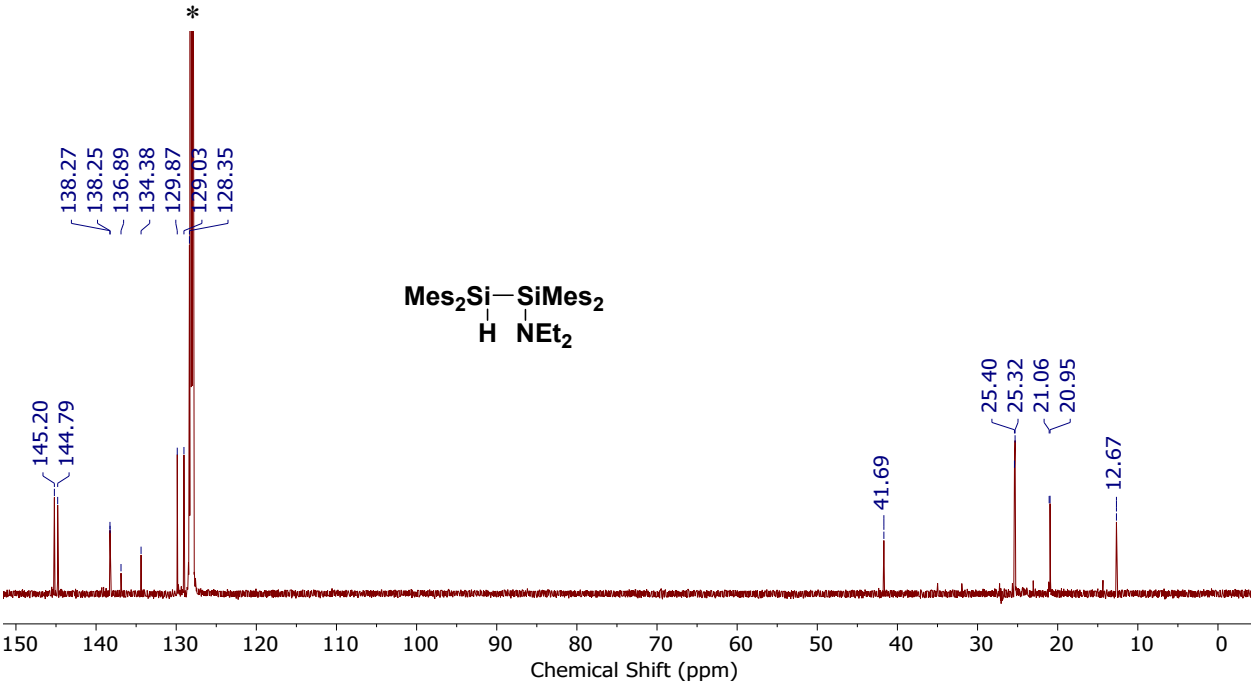

Figure S14 ^{13}C{^{1}H} NMR spectrum (151 MHz, C_6D_6) of **7**. The signal denoted with * is the solvent C_6D_6.

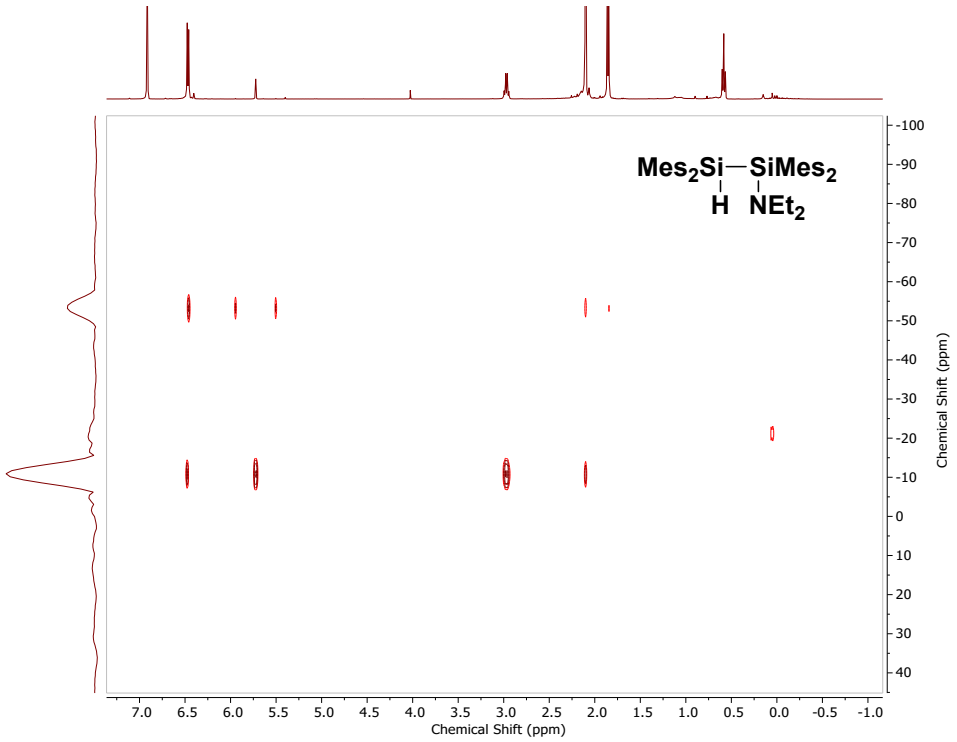

Figure S15 ^{1}H-^{29}Si gHMBC spectrum (C_6D_6) of **7**.

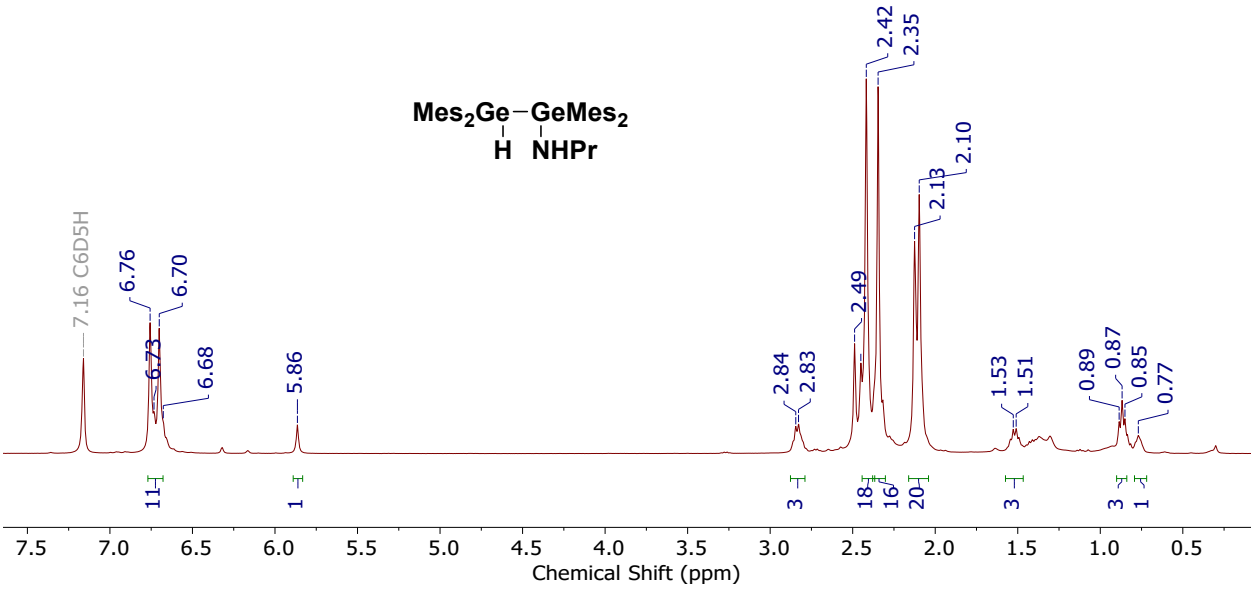

Figure S16 ^{1}H NMR spectrum (600 MHz, C_6D_6) of crude **8**. The second set of signals are consistent with 1,1,2,2-tetramesityldigermanol.[4]

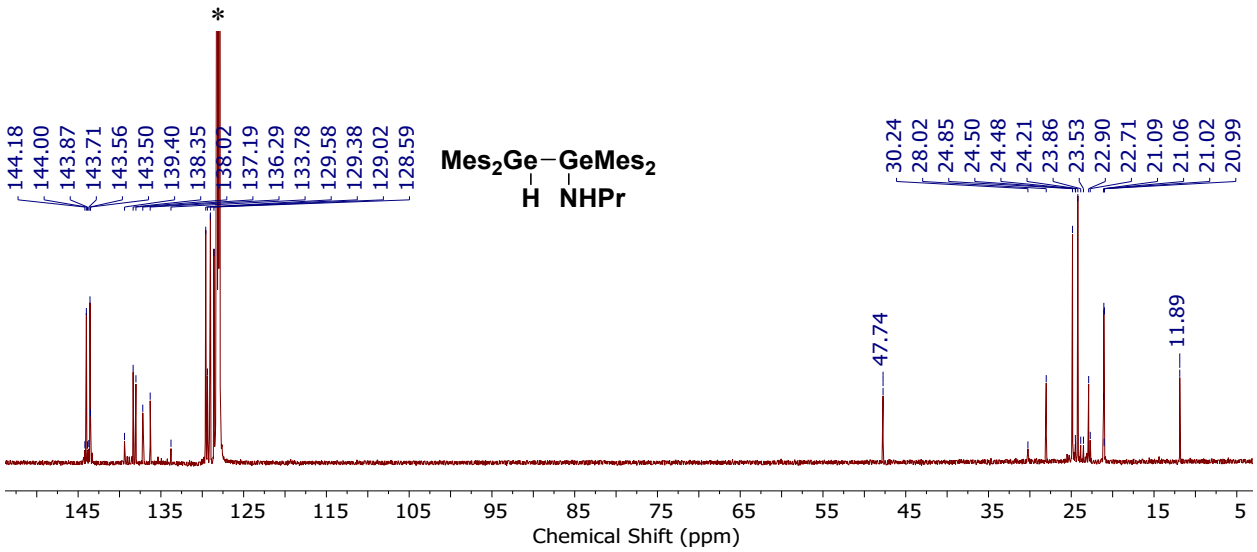

Figure S17 $^{13}C\{^{1}H\}$ NMR spectrum (151 MHz, C_6D_6) of crude **8**. The signal denoted with * is the solvent C_6D_6.

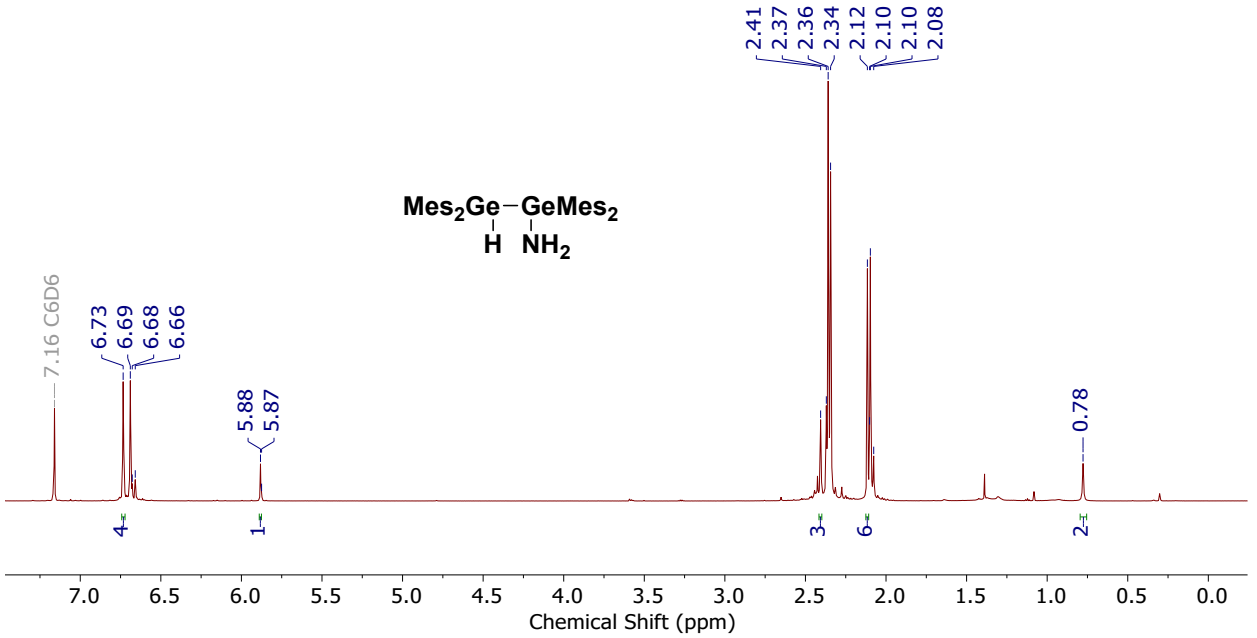

Figure S18 ^{1}H NMR spectrum (600 MHz, C_6D_6) of crude **9**. 1,1,2,2-Tetramesityldigermanol[4] can also be observed in the spectrum.

X-Ray Crystallography

Data Collection and Processing. Although **3** was most often obtained as a pale-yellow oil, on one occasion a crystal of the sample was obtained after 3 months. The sample was mounted on a Mitegen polyimide micromount with a small amount of Paratone N oil. All X-ray measurements were made on a Bruker Kappa Axis Apex2 diffractometer at a temperature of 110 K. The unit cell dimensions were determined from a symmetry constrained fit of 2497 reflections with 4.9° < 2θ < 44.0°. The data collection strategy was a number of ω and φ scans which collected data up to 48.84° (2θ). The frame integration was performed using SAINT.[7] The resulting raw data were scaled and absorption corrected using a multi-scan averaging of symmetry equivalent data using SADABS.[8]

Structure Solution and Refinement. The structure was solved by using a dual space methodology using the SHELXT program.[9] All non-hydrogen atoms were obtained from the initial solution. The hydrogen atoms were introduced at idealized positions and were treated in a mixed fashion. The hydrogen atoms attached to Si2 and N1 were found in the difference map and were allowed to refine isotropically. The structural model was fit to the data using full matrix least-squares based on F^2. The calculated structure factors included corrections for anomalous dispersion from the usual tabulation. The structure was refined using the SHELXL-2014 program from the SHELXTL suite of crystallographic software.[10] Graphic plots were produced using the XP program suite.[11] Additional information and other relevant literature references can be found in the reference section of this website (http://xray.chem.uwo.ca)

Table S1 Summary of Crystal Data for **3**

Formula	$C_{39}H_{53}NSi_2$
CCDC #	2025827
Formula Weight (*g/mol*)	592.00
Crystal Dimensions (*mm*)	0.243 × 0.057 × 0.055
Crystal Color and Habit	colourless prism
Crystal System	Triclinic
Space Group	P -1
Temperature, K	110
a, Å	11.803(6)
b, Å	12.244(7)
c, Å	12.493(6)
α,°	86.15(3)
β,°	88.39(3)
γ,°	70.61(2)
V, Å^3	1699.2(16)
Number of reflections to determine final unit cell	2497
Min and Max 2θ for cell determination, °	4.9, 44.0

Z	2
F(000)	644
ρ (*g/cm*)	1.157
λ, Å, (MoKα)	0.71073
μ, (cm^{-1})	0.132
Diffractometer Type	Bruker Kappa Axis Apex2
Scan Type(s)	phi and omega scans
Max 2θ for data collection, °	48.84
Measured fraction of data	0.995
Number of reflections measured	24512
Unique reflections measured	5581
R_{merge}	0.0857
Number of reflections included in refinement	5581
Cut off Threshold Expression	I > 2sigma(I)
Structure refined using	full matrix least-squares using F^2
Weighting Scheme	$w=1/[sigma^2(Fo^2)+(0.0783P)^2+0.8302P]$ where $P=(Fo^2+2Fc^2)/3$
Number of parameters in least-squares	399
R_1	0.0606
wR_2	0.1424
R_1 (all data)	0.1094
wR_2 (all data)	0.1655
GOF	1.020
Maximum shift/error	0.000
Min & Max peak heights on final ΔF Map (e^-/Å)	-0.365, 0.567

Where:

$R_1 = \Sigma(|F_o| - |F_c|) / \Sigma F_o$

$wR_2 = [\Sigma(w(F_o^2 - F_c^2)^2) / \Sigma(w F_o^4)]^{½}$

GOF = $[\Sigma(w(F_o^2 - F_c^2)^2) / (\text{No. of reflns. - No. of params.})]^{½}$

Additional Schemes and Figures for the Discussion

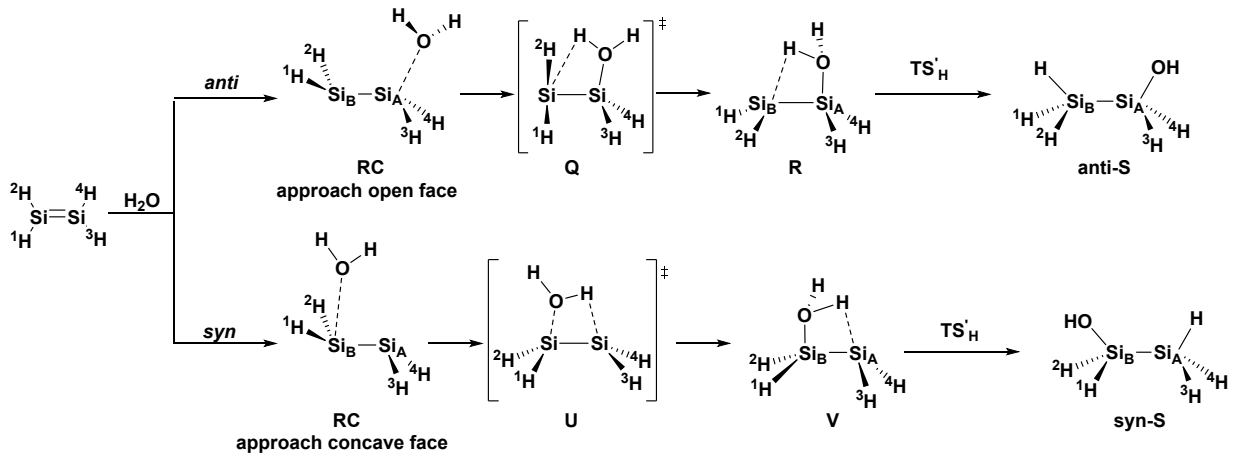

Scheme S1 Modified mechanisms for the addition of water to disilene

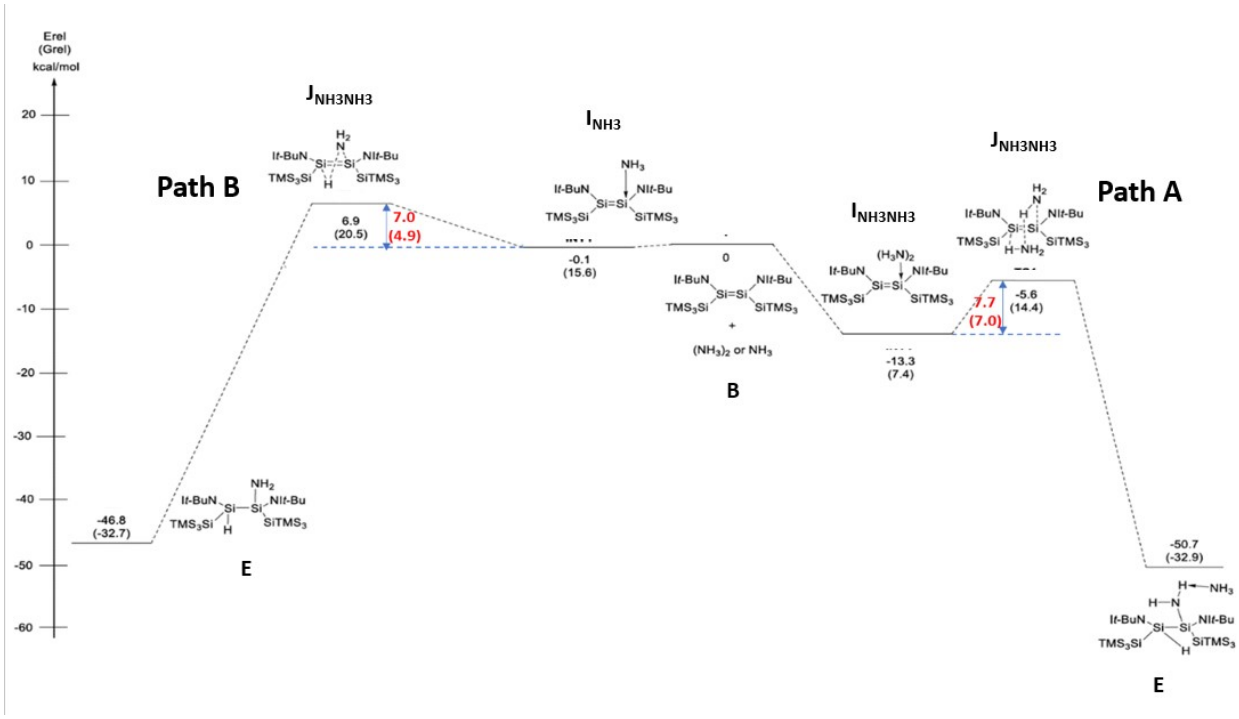

Figure S19 The reaction pathways proposed by Wendel *et al*. for the addition of ammonia to disilene **B** to yield **E**.[12] (Reaction energy profile was adapted from Scheme S1 in reference 12 and reprinted with permission from J. Wiley & Sons.)

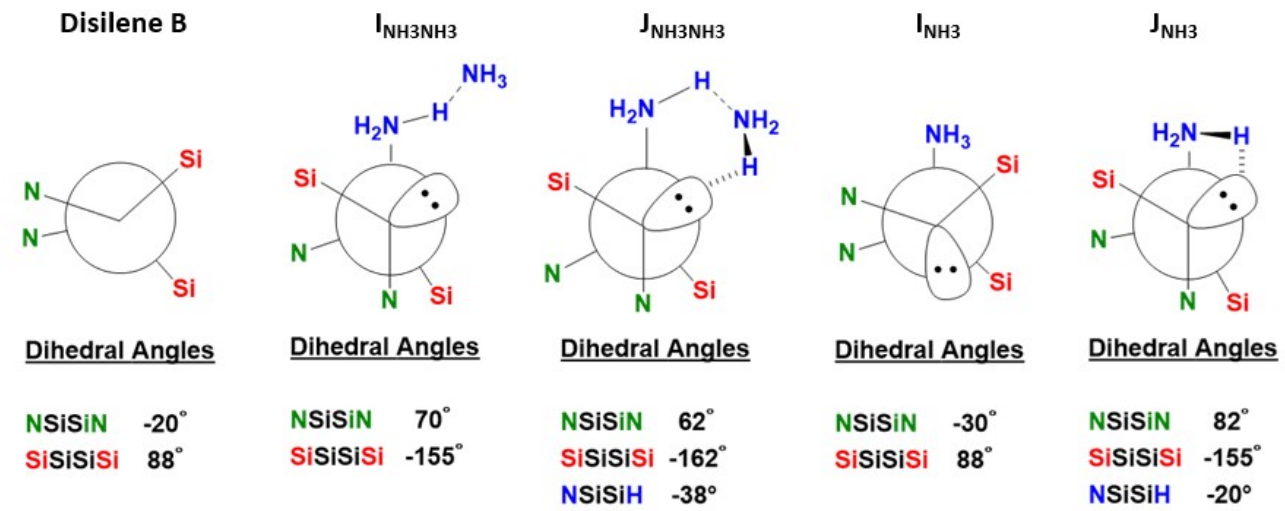

Figure S20 Newman projections for species along Path A and Path B (Scheme 2a).[12]

Computations

Computational Methodology

Calculations were done using the Gaussian 16[13] program package. The geometries of all stationary points and transition states on the potential energy surfaces of the proposed pathways were optimized at M06-2X/6-311+G(d,p) computational level. Transition states were located by executing standard transition state optimizations. Frequency computations were performed to characterize the nature of transition states (one imaginary frequency) and the local minima (no imaginary frequency) at the same computational level. Intrinsic reaction coordinate (IRC)[14] calculations for the transition states optimized using the standard method were also carried out at the same level to connect the transition states to the reactants and products. Solvent effects were investigated by performing single point energy computations at the same computational level using the Integral Equation Formalism-Polarizable Continuum Model (IEF-PCM)[15] and benzene as the solvent. To compute zero-point corrected electronic energy and Gibbs energy values in the solvent phase, thermodynamic corrections at 298 K obtained from the frequency calculations were added to the electronic energy obtained from single point IEF-PCM computations.

Reaction Path involving the Direct Formation of a *syn*-donor adduct, syn-10 (Path 1)

In the computations of Path 1, it should be noted that the structure of **TS(RC|syn-10)** was optimized under the constraint of the N – Si bond distance, and not fully. Moreover, attempts to optimize the structure of **TS(RC|syn-10)** with no constraints using M062X produced the transition state structure for the formation *anti*-donor adduct. In order to test the DFT functional, **TS(RC|syn-10)** was also fully optimized at the B3LYP/6-311+G(d,p) level of theory. The B3LYP-computed Gibbs free activation barrier was found to be 23 kcal/mol (Figure S21), which is even higher than free energy barrier computed with the M062X functional.

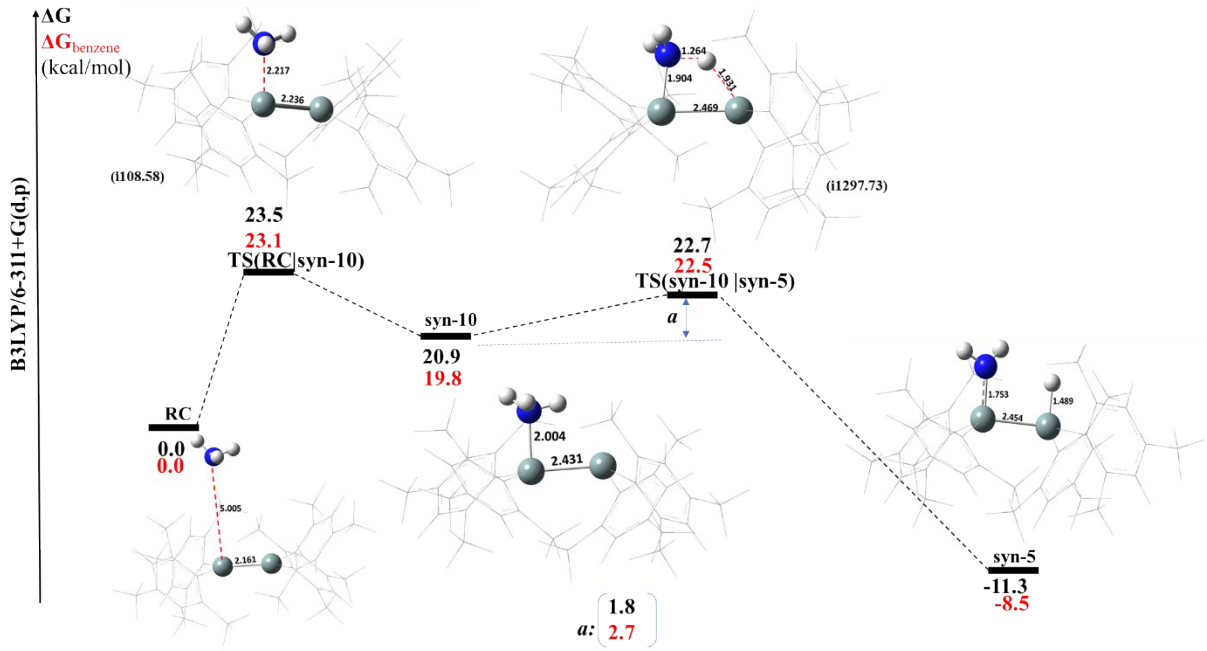

Figure S21 Free energy diagram of Path S1 computed with B3LYP.

Scan and IRC Computations

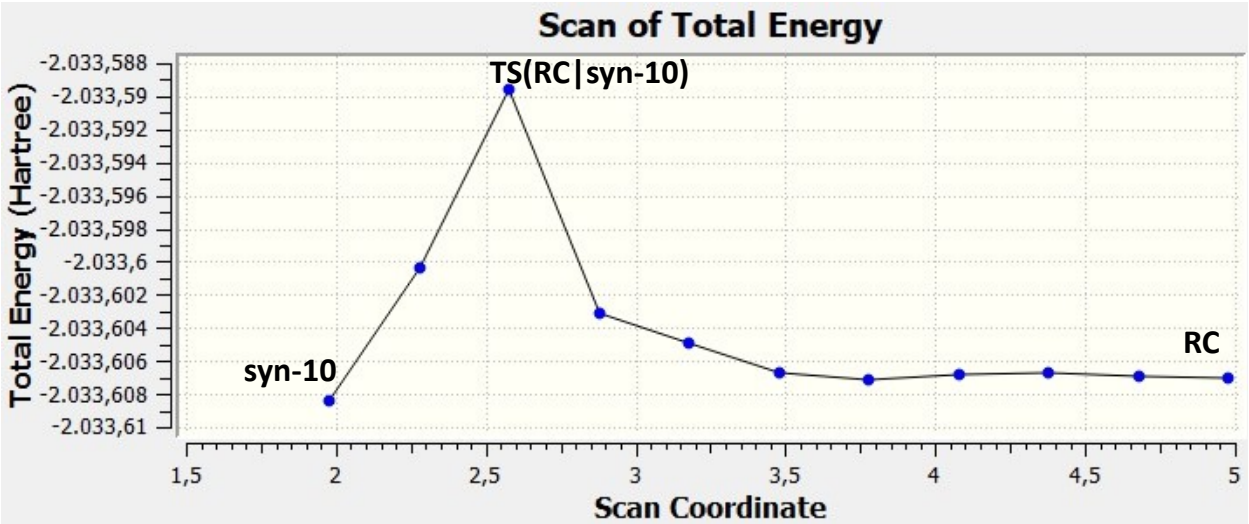

Figure S22 Potential energy scan for transition state **TS(RC|syn-10).**

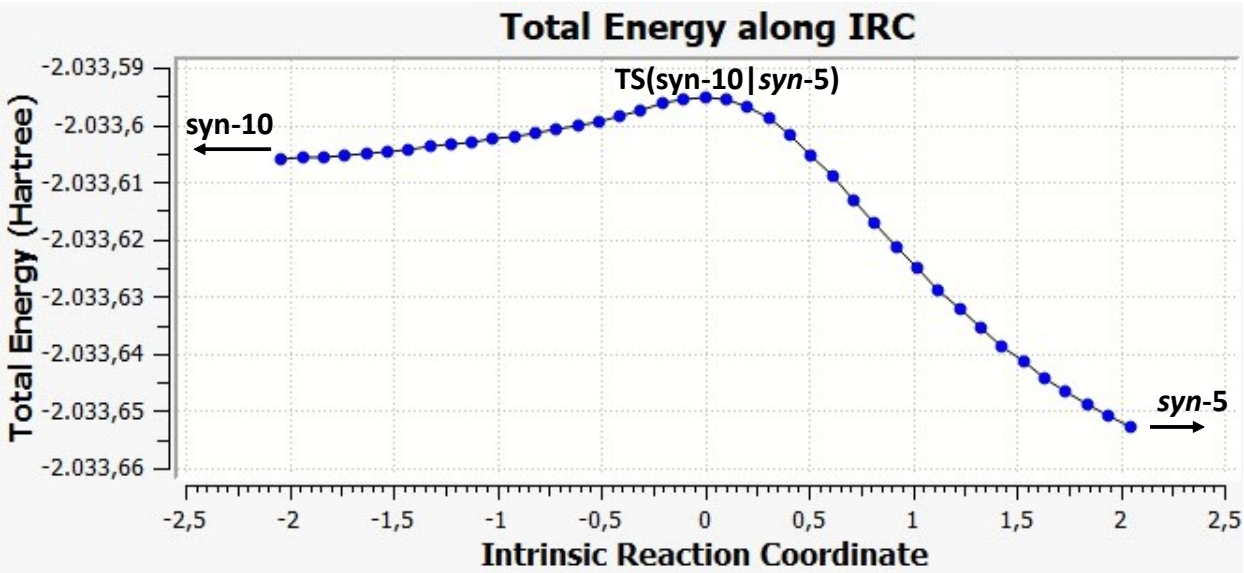

Figure S23 IRC for transition state **TS(syn-10|syn-5).**

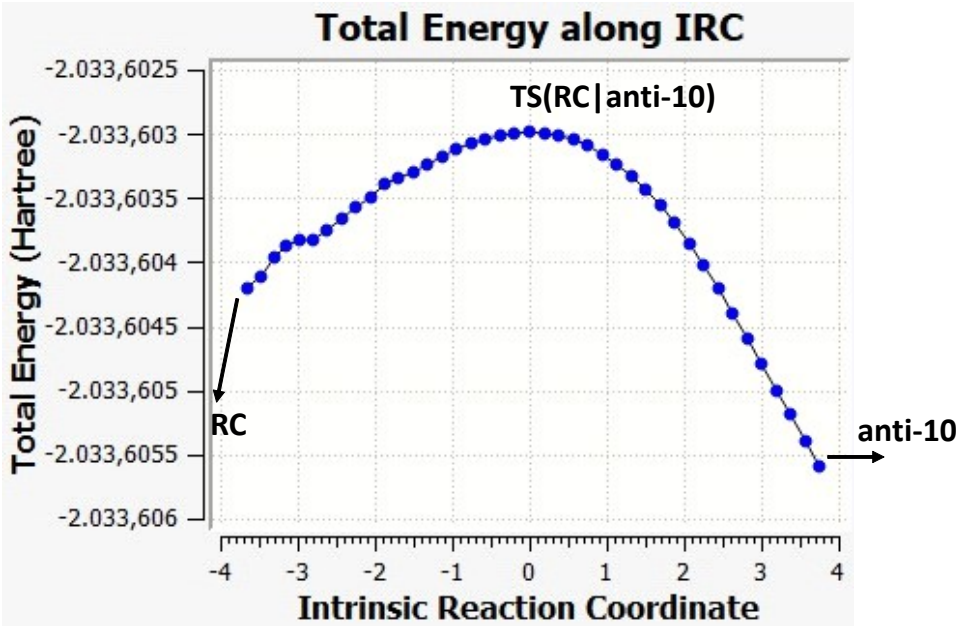

Figure S24 IRC for transition state **TS(RC|anti-10).**

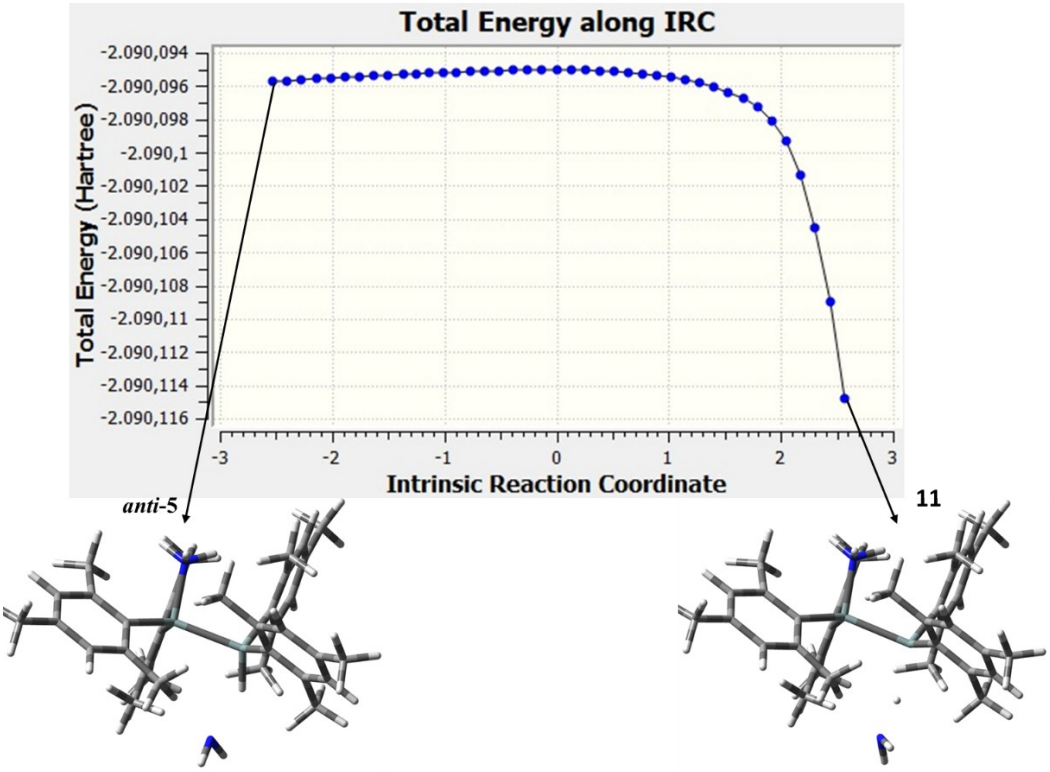

Figure S25 IRC for transition state **TS(11|protonated-anti-5)**.

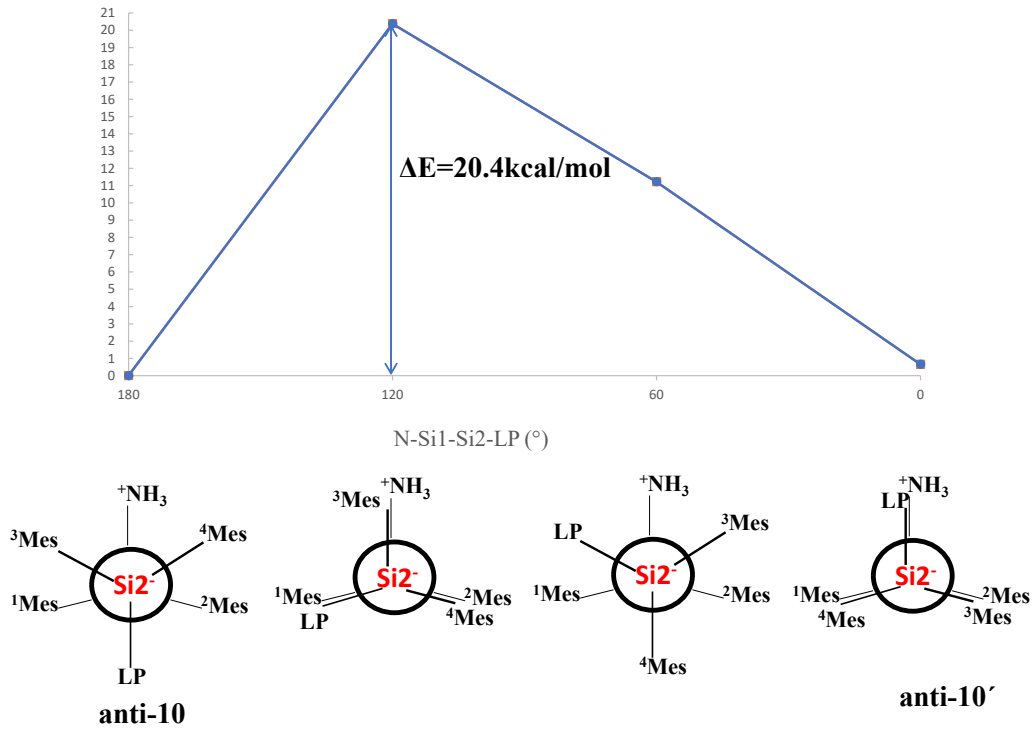

Figure S26 Energy profile (kcal/mol) for the Si – Si bond rotation from **anti-10** to **anti-10´.**

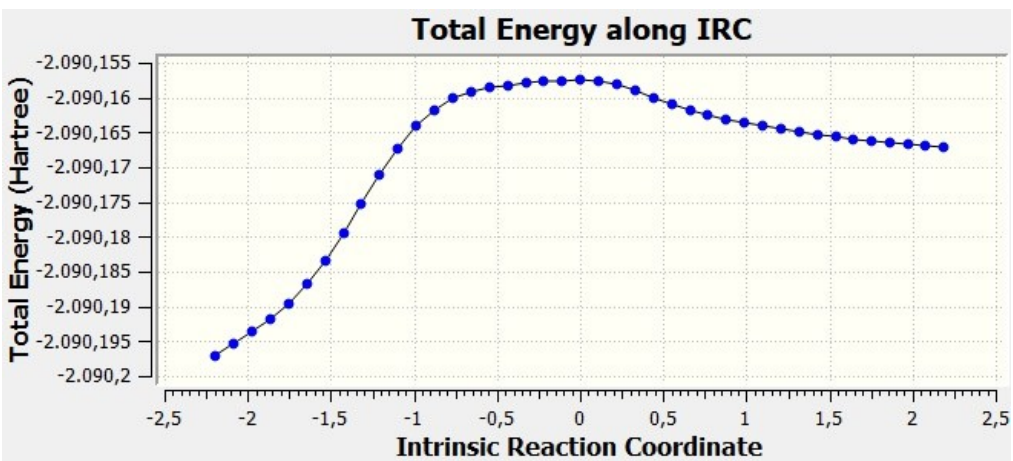

Figure S27 IRC for transition state **TS(syn12|syn-5)**.

Energies

Absolute energies of all stationary points and transition states are listed below.

Table S2. Electronic and Gibbs energies (au) and number of imaginary frequencies (NIMAG) for all structures in the suggested pathways computed with M062x/6-311+G(d,p) computational level.

	E	G	NIMAG
NH_3	-56.511221	-56.529247	0
1	-1976.354323	-1976.433178	0
RC	-2032.871347	-2032.957565	0
TS(RC|syn-10)	-2032.851712	-2032.927704	1 (180.45i)
syn-10	-2032.867563	-2032.941509	0
TS(syn-10|syn-5)	-2032.860580	-2032.935099	1 (1394.10i)
syn-5	-2032.934477	-2033.011220	0
TS(RC|anti-10)	-2032.865899	-2032.945161	1 (91.99i)
anti-10	-2032.867783	-2032.944444	0
11	-2089.387073	-2089.469338	0
TS(11|protonated-anti-5)	-2089.322967	-2089.402526	1 (131.35i)
***anti*-5**	-2032.945350	-2033.022275	0
TS(anti-10|syn-10)	-2032.858221	-2032.936983	1 (108.14i)
RC-D	-2089.388946	-2089.474029	0
TS(RC-D|anti-12)	-2089.386147	-2089.467922	1 (98.76)
anti-12	-2089.396577	-2089.476074	0
TS(anti-12|syn-12)	-2089.382716	-2089.464451	1 (117.92i)
syn-12	-2089.391390	-2089.473456	0
TS(syn-12|syn-5)	-2089.384819	-2089.463537	1 (711.02i)
syn-5 + NH_3	-2089.450994	-2089.534131	0

Table S3. Electronic and Gibbs energies (au) and number of imaginary frequencies (NIMAG) computed with B3LYP/6-311+G(d,p) computational level for all structures in Path S1.

	E	G	NIMAG
RC	-2033.602211	-2033.69579	0
TS(RC|syn-10)	-2033.576322	-2033.65834	1 (108.58i)
syn-10	-2033.579851	-2033.66251	0
TS(syn-10|syn-5)	-2033.577654	-2033.65974	1 (1297.73i)
syn-5	-2033.649654	-2033.73076	0

Cartesian coordinates for all structures are given in the accompanying .xyz file.

References

[1] M. J. Fink, M. J. Michalczyk, K. J. Haller, J. Michl, R. West, *Organometallics*, 1984, **3**, 793 – 800.
[2] a) W. Ando, T. Tsumuraya, *J. Chem. Soc., Chem. Commun.*, 1987, 1514 – 1515; b) T. Tsumuraya, Y. Kabe, W. Ando, *J. Organomet. Chem.*, 1994, **482**, 131 – 138.
[3] K. L. Hurni, P. A. Rupar, N. C. Payne, K. M. Baines, *Organometallics*, 2007*,* **26***,* 5569 – 5575.
[4] K. M. Baines, J. A. Cooke, C. E. Dixon, H. W. Liu, M. R. Netherton, *Organometallics*, 1994*,* **13***,* 631 – 634.
[5] J. Luijten, F. Rijkens, G. V. D. Kerk, *Adv. Organomet. Chem*, 1966, **3**, 397 – 446.
[6] a) D. A. Armitage, R. J. P. Corriu, T. C. Kendrick, B. Parbhoo, T. D. Tilley, J. W. White, J. C. Young. *The Silicon-Heteroatom Bond,* John Wiley & Sons, West Sussex, 1991; b) U. Wannagat, *Biochemistry of Silicon and Related Problems,* ed. G. Bendz, I. Lindqvist, V. Runnström-Reio, Springer, Boston, ch. The Silicon-Nitrogen Bond, 1978, pp 77 – 90.
[7] Bruker-AXS, SAINT version 2013.8, 2013, Bruker-AXS, Madison, WI 53711, USA.
[8] Bruker-AXS, SADABS version 2012.1, 2012, Bruker-AXS, Madison, WI 53711, USA.
[9] G. M. Sheldrick, *Acta Cryst*., 2015, **A71**, 3 – 8.
[10] G. M. Sheldrick, *Acta Cryst*., 2015, **C71**, 3 – 8
[11] Bruker-AXS, XP version 2013.1, 2013, Bruker-AXS, Madison, WI 53711, USA.
[12] D. Wendel, T. Szilvási, D. Henschel, P. J. Altmann, C. Jandl, S. Inoue, B. Rieger, *Angew. Chem. Int. Ed*., 2018, **57**, 14575 – 14579.
[13] M. J. Frisch, G. W. Trucks, H. B. Schlegel, G. E. Scuseria, M. A. Robb, J. R. Cheeseman, G. Scalmani, V. Barone, G. A. Petersson, H. Nakatsuji, X. Li, M. Caricato, A. V. Marenich, J. Bloino, B. G. Janesko, R. Gomperts, B. Mennucci, H. P. Hratchian, J. V. Ortiz, A. F. Izmaylov, J. L. Sonnenberg, D. Williams-Young, F. Ding, F. Lipparini, F. Egidi, J. Goings, B. Peng, A. Petrone, T. Henderson, D. Ranasinghe, V. G. Zakrzewski, J. Gao, N. Rega, G. Zheng, W. Liang, M. Hada, M. Ehara, K. Toyota, R. Fukuda, J. Hasegawa, M. Ishida, T. Nakajima, Y. Honda, O. Kitao, H. Nakai, T. Vreven, K. Throssell, J. A. Montgomery, Jr., J. E. Peralta, F. Ogliaro, M. J. Bearpark, J. J. Heyd, E. N. Brothers, K. N. Kudin, V. N. Staroverov, T. A. Keith, R. Kobayashi, J. Normand, K. Raghavachari, A. P. Rendell, J. C. Burant, S. S. Iyengar, J. Tomasi, M. Cossi, J. M. Millam, M. Klene, C. Adamo, R. Cammi, J. W. Ochterski, R. L. Martin, K. Morokuma, O. Farkas, J. B. Foresman, and D. J. Fox, Gaussian, Inc., Wallingford CT, 2016.
[14] a) K. Fukui, *Acc. Chem. Res.*, 1981, **14**, 363 – 368; b) H. P. Hratchian and H. B. Schlegel, in *Theory and Applications of Computational Chemistry: The First 40 Years*, Ed. C. E. Dykstra, G. Frenking, K. S. Kim, G. Scuseria (Elsevier, Amsterdam, 2005) 195 – 249.
[15] G. Scalmani, M. J. Frisch, *J. Chem. Phys.*, 2010, **132**, 114110.